Journal of Industrial and Production Engineering

ISSN: (Print) (Online) Journal homepage: https://www.tandfonline.com/loi/tjci21

Hierarchical energy optimization management of active distribution network with multi-microgrid system

Sun Wenzhi, Huijuan Zhang, Ming-Lang Tseng, Zhang Weipeng & Li Xinyang

To cite this article: Sun Wenzhi, Huijuan Zhang, Ming-Lang Tseng, Zhang Weipeng & Li Xinyang (2022) Hierarchical energy optimization management of active distribution network with multi-microgrid system, Journal of Industrial and Production Engineering, 39:3, 210-229, DOI: 10.1080/21681015.2021.1972478

To link to this article: https://doi.org/10.1080/21681015.2021.1972478

JOURNAL OF INDUSTRIAL AND PRODUCTION ENGINEERING
2022, VOL. 39, NO. 3, 210–229
https://doi.org/10.1080/21681015.2021.1972478

Taylor & Francis
Taylor & Francis Group

ARTICLE

Hierarchical energy optimization management of active distribution network with multi-microgrid system

Sun Wenzhi[a,b], Huijuan Zhang[a,b], Ming-Lang Tseng[c,d,e], Zhang Weipeng[f] and Li Xinyang[a]

[a]State Key Laboratory of Reliability and Intelligence of Electrical Equipment, Hebei University of Technology, Tianjin, China; [b]Key Laboratory of Electromagnetic Field and Electrical Apparatus Reliability of Hebei Province, Hebei University of Technology, Tianjin, China; [c]Institute of Innovation and Circular Economy, Asia University, Taiwan; [d]Department of Medical Research, China Medical University Hospital, China Medical University, Taichung, Taiwan; [e]Faculty of Economics and Management, University Kebangsaan Malaysia, Malaysia; [f]Tianjin Chengxi District Power Supply Company, Tianjin, China

ABSTRACT

A hierarchical energy optimization management model is established and a multi-microgrid operation strategy that mixes the battery and the power interaction designed to strengthen the system output capability. This study carries out dynamic optimization to achieve optimal economic benefits of active distribution network with multi-microgrid system. An improved sparrow search algorithm is developed to achieve an optimal energy configuration by integrating Bernoulli chaotic mapping, Lévy flight, mutation, crossover and competition. The superiority of the improved sparrow search algorithm is demonstrated by the results of different test functions and evaluation indicators. The effectiveness of the proposed method is verified by solving and analyzing the optimal configuration of energy management model. Case study results reveal that the active distribution network with multi-microgrid system has good economic and environmental benefits under various scenarios. The methods proposed are of great significance for the economic operation and environmental protection of multi-microgrid active distribution network.

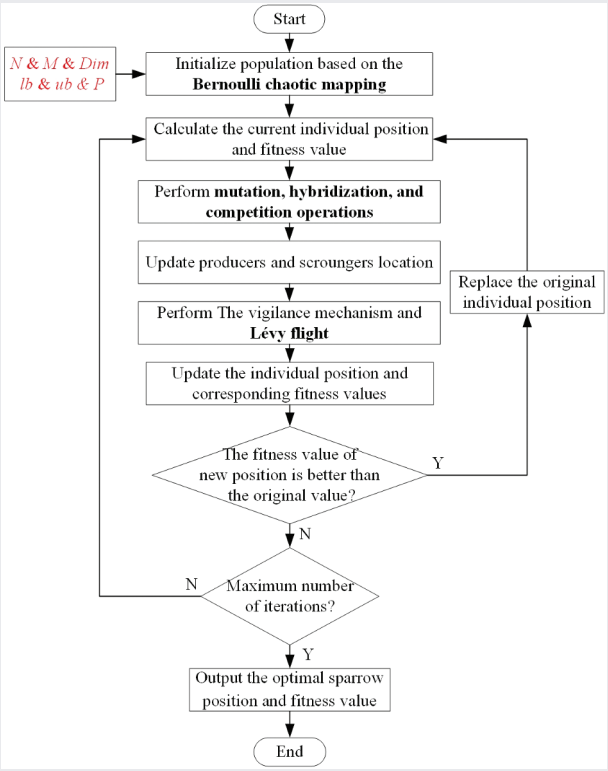

ARTICLE HISTORY
Received 08 May 2021
Revised 22 July 2021
Accepted 20 August 2021

KEYWORDS
Active distribution network; multi-microgrid; renewable energy; improved sparrow search algorithm; hierarchical energy optimization management

CONTACT Ming-Lang Tseng tsengminglang@gmail.com Institute of Innovation & Circular Economy, Asia University, Taichug, Taiwan

1. Introduction

With the rapid development of human society, the problems caused by the energy crisis have become increasingly prominent in recent years [1–3]. Under environment protection, the use of clean energy such as wind energy and solar energy has developed rapidly [4,5]. The microgrid (MG) system based on wind power generation system and photovoltaic power generation system has become an effective means to manage the distributed generation (DG) because the uncertainty of the DG with renewable energy [6–8]. The output stability of power generation system is improved to a certain extent by MG, and self-control and protection is realized by utilizing the complementary characteristics between wind and solar resources and combining with the power control strategy of power generation system [9,10]. An effective energy optimization management model is usually with hierarchy structure and a multi-microgrid (MMG) operation strategy needs to design to mix the battery and power interaction designed to strengthen the system output capability.

As a large number of independent microgrids are connected to the Active distribution network (ADN), a complex ADN with MMG system is gradually formed [11]. The ADN adopts a more flexible network topology to actively manage the local DG due to the rapid development of distributed power generation technology and microgrid technology [12,13]. In the high coupling and complexity of the MMG system, emerging optimization algorithms may achieve a faster optimization process for power scheduling arrangement [14], and the intelligent optimization algorithms in solving various complex problems of microgrid system operation have been studied for achieving the optimization development [15]. The sparrow search algorithm (SSA) is a new heuristic method inspired using sparrow foraging and vigilance behaviors [16], and various improved algorithms are beginning to be used for energy optimization management [17, 18].

A reasonable power distributed supply is needed with a large amount of clean energy entering the MMG system [19]. The capacity configuration of the DG inside the system affects a series of issues such as economic cost, environmental pollution and operational reliability [20]. Therefore, reasonable optimization of the ADN with MMG system based on intelligent optimization algorithms is meaningful. It helps to actually adjust the dispatch plan of the entire network, effectively reduce the energy fluctuation caused by renewable energy output and improve the quality of power supply and effectively reduce the operating cost and improve the clean energy utilization.

The main contributions of this study are as follows. (1) An improved sparrow search algorithm (ISSA) is proposed by introducing the Bernoulli chaotic mapping, Lévy flight and the operations of mutation, crossover and competition to develop the global search capability of the original SSA, and different classical test functions are used to test the various ability of the proposed ISSA; (2) The ADN model with MMG system is divided into the MMG system layer and the ADN layer, and adaptive weight coefficients are used to transform the multi-objective problem into a single-objective problem under dynamic programming; (3) A MMG operation strategy is proposed for strengthening the power supply capacity of the system; and (4) The performance of ISSA in the practical application is verified by considering the economic and environmental benefits in the ADN with MMG system.

The remaining sections are arranged as follows. Section 2 reviews traditional energy optimization management strategies in the MMG system. Section 3 introduces the principle of the ISSA and verifies its performance. Section 4 describes the structure of the ADN with MMG system model based on ISSA for energy optimization management. Section 5 is a case study. Section 6 is the main innovation of this study and its impact on industry, environment and society. Some meaningful conclusions and future work direction are summarized in Section 7.

2. Literature review

The energy management of the MMG system is mainly divided into two structures, i.e., centralized structure and distributed structure [21]. The centralized structure uses a control strategy to communicate with each microgrid central controller (MGCC) and the underlying electrical equipment, and sends control commands. The distributed structure relies on a multi-agent system for operation management and decision-making, and realizes stable operation of the MMG system through communication and coordination among agents [6, , 22]. To achieve the coordination and optimization of the distribution network and the MMG system, bi-level programming theory is gradually used to connect the distribution network to distributed power sources through MMG system[23, 24].

In the hierarchical energy optimization management model, the independent microgrid system usually takes its own cost as the optimization goal, and finally makes the MMG system obtain the overall profit [6,25,26]. 3,proposed a bi-level coordinated control model for the energy management optimization of the ADN with MMG. The lowest operating cost is the optimization goal of the low-level model. The output of the microgrid equipment is reasonably allocated, and the control of the upper-level model is realized. 27,proposed a bi-level distributed optimized operation method for interconnected microgrid system. The interconnected microgrid system of the upper level

optimizes the trading power with microgrids to maximize revenue, and the lower level optimizes the output and energy storage of distributed energy sources with the goal of lowest cost. In addition to the system cost, the evaluation indicators of the microgrid system also include transmission efficiency, power quality and system reliability [28–30]. 31,proposed a distributed voltage control model and control strategy based on a new network partition method to solve the capacity curves of distributed power sources and the stability of the energy storage system. 32,took the minimum network loss as the goal of the upper model, which realized the optimal power distribution of the microgrid, and reduced the power consumption of the energy mutual assistance between microgrids.

Intelligent optimization algorithms are crucial methods to maximize the benefit of the operation scheduling. 33, used particle swarm optimization to optimally dispatch the distributed microgrid, which minimized carbon emissions and the cost of each microgrid. 34, improved the shuffled complex evolution algorithm, making it a multi-objective optimization algorithm with a higher coverage rate and a higher search success rate, and used for the energy optimization management. 35, proposed a multi-dimensional firefly algorithm used to solve the day-ahead scheduling optimization problem in the microgrid, and it is concluded that multi-dimensional firefly algorithm exhibited high performance in terms of convergence speed and reliability of optimization through comparative analysis.

In this process, existing research is mostly aimed at optimizing the internal operation of the system, while there are few studies on the energy interaction of the hierarchical structure, and the improvement of the operating strategy is neglected. In addition, the performance of the intelligent optimization algorithm itself has an important impact on the final optimization result, and the algorithm used has problems such as slow convergence speed and easy to fall into local convergence. Aiming at solving the above problems, this study develops the ISSA to optimize the ADN with MMG system. The Bernoulli chaotic mapping, Lévy flight and the operations of mutation, crossover and competition are integrated to the traditional sparrow search algorithm for further improving its global search capability. In addition, an MMG operation strategy with energy storage system and the ability to interact with the power grid is proposed to consolidate the MMG system output capability. The experimental results verify the superiority of the proposed algorithm and the effectiveness of the proposed strategy. This study effectively ensures the operation stability of microgrid, and brings both good economic and environmental benefits.

3. Model of improved sparrow search algorithm

The principles of the original sparrow search algorithm and the ISSA are mainly introduced section.

3.1. Sparrow search algorithm

Producers and beggars are important components of the SSA model. Producers tend to have high energy reserves and are responsible for finding rich food source areas. The energy reserve represents the fitness value of sparrows. The producers provide foraging directions for the beggars who join later to obtain better fitness values. In addition, if the beggars who join later can find better food sources, they become producers. The identities of producers and beggars in the population change dynamically, and the sum of their numbers remains constant. Beggars monitor the feed of producers and nearby areas in a reasonable manner. In addition, alerting mechanisms were added in the late foraging period to prevent predators from attacking. In SSA, an n-row d-dimensional variable matrix is used as an optimized space with sparrows. The position of sparrows is expressed as follows.

$$X = \begin{bmatrix} x_{1,1} & x_{1,2} & \cdots & x_{1,d} \\ x_{2,1} & x_{2,2} & \cdots & x_{2,d} \\ \cdots & \cdots & \cdots & \cdots \\ x_{n,1} & x_{n,2} & \cdots & x_{n,d} \end{bmatrix} \tag{1}$$

The producer usually accounts for 20% of the total number of sparrows, and the position updates as:

$$X_{i,j}^{m+1} = \begin{cases} X_{i,j}^{m} * \exp(\frac{-i}{\alpha * M_{\max}}) R_2 < ST \\ X_{i,j}^{m} + Q * L R_2 \geq ST \end{cases} \tag{2}$$

where m indicates the current iteration number. $X_{i,j}^{m}$ is the value of the i-th sparrow in the j-th dimension, $j = 1,2, \ldots, d$. $M_{\max}$ is the maximum number of iterations. Q represents a random value in a normal distribution. L is a matrix of size $1 \times d$ for which element inside is one. $R_2 \in [0, 9]$ is the warning value. $ST \in [0.5, 1]$ is the safe value. When the warning value is less than the safety value, it indicates no predators appear around. Then, the producer can search the safe areas with higher fitness values. On the contrary, if the warning value is greater than the safe value, the population needs to fly to other safe areas as predators may appear there.

The remaining sparrows serve as scroungers, and their locations update as:

$$X_{i,j}^{m+1} = \begin{cases} Q * \exp(\frac{X_{\mathrm{w}}^{t} - X_{i,j}^{t}}{i^2}) i > n/2 \\ X_{\mathrm{b}}^{m+1} + \left| X_{i,j}^{m} - X_{\mathrm{b}}^{m+1} \right| * A^{+} * L \text{otherwise} \end{cases} \tag{3}$$

where X_b is the optimal position of the discoverer under the current iteration number. X_w is the worst position in the current population. $A^+ = A^T(AA^T)^{-1}$, where A is a matrix of size $1 \times d$ for which internal element randomly takes the value 1 or −1. When $i > n/2$, these sparrows are extremely hungry, and their fitness values are poor. Therefore, their foraging positions need to change to obtain higher energy.

Assume that vigilant sparrows account for 10% to 20% of the total population, and such sparrows is randomly generated among individuals in the population. The position update Eq. is expressed as:

$$X_{i,j}^{m+1} = \begin{cases} X_b^m + \beta * (X_{i,j}^m - X_b^m) \text{otherwise} \\ X_{i,j}^m + K * \left(\frac{|X_{i,j}^m - X_w^m|}{(f_i - f_w) + \sigma}\right) f_i = f_b \end{cases} \quad (4)$$

where β is the step length control parameter that is a random value, a mean as 0 and a variance as 1, under a normal distribution. $K \in [-1, 1]$ is a random value, which is used to control the sparrow moving direction. σ is a very small constant used to prevent the denominator from being zero. f_w and f_b represent the worst and best individual fitness values in the current population, respectively. f_i represents the fitness value of the i-th sparrow. When $f_i = f_b$, the individual sparrow is located in the center of the entire population. Other individual sparrows can approach it in time when facing the danger of predators. However, sparrow individuals located at the edge of the population need to move closer to the optimal position, being away from predators.

3.2. Improvement of sparrow search algorithm

The proposed ISSA model is developed to resolve the problems such as easily falling into a local minimum and slow convergence speed. First, a Bernoulli chaotic mapping is added to the population initialization to improve the spatial distribution of the initial sparrow population. Secondly, the mutation, hybridization and competition strategies in the differential evolution algorithm (DE) are used to enhance the sparrow's diversity and randomness during the foraging process. Finally, the sparrow in the central position performs Lévy flight process to update its current position to explore a better position, thus achieving the global optimal solution in the later stage.

3.2.1. Bernoulli chaotic mapping

The chaotic mapping is used to replace the random generation number, and the chaotic sequence has the characteristics of nonlinearity, ergodicity and unpredictability. Several chaotic mapping analyses with parameters settings can refer to [36].

Figure 1 showed the uniformity of Bernoulli chaotic mapping is found better. To improve the spatial distribution of sparrows and enhance the global optimal solution, the Bernoulli chaotic mapping is selected to initialize the population. The Bernoulli chaotic mapping Eq. is given as follows.

$$r_{n+1} = \begin{cases} r_n/(1-p) r_n \in (0, 1-p] \\ (r_n - 1 + p)/p r_n \in (1-p, 1) \end{cases} \quad (5)$$

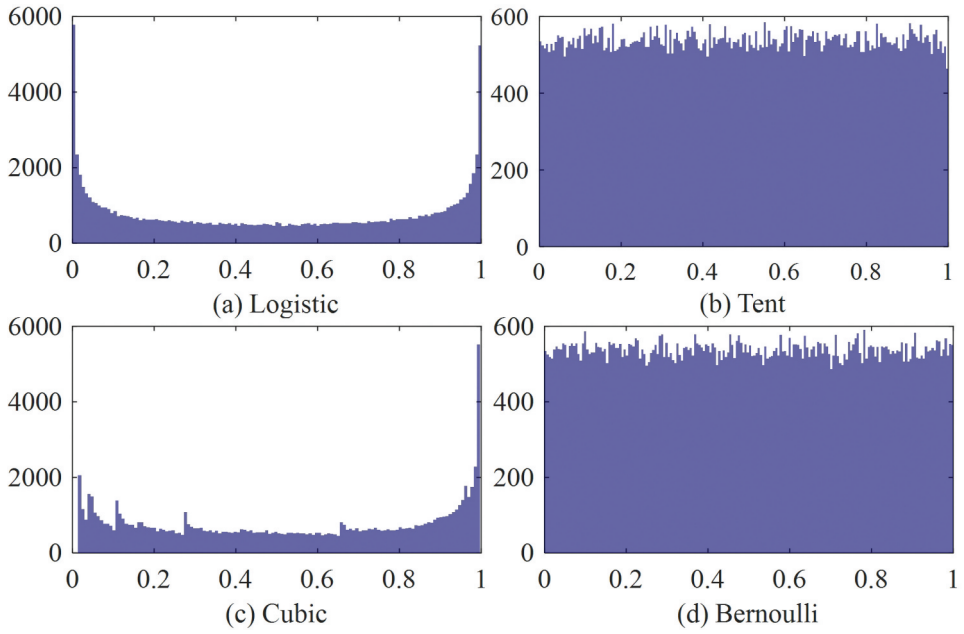

Figure 1. The histograms of chaotic mappings under the same iteration number.

where rn is the n-th chaotic number. p is a chaotic parameter. The steps for population initialization are listed as follows.

(1) Set parameter (p) and maximum iteration number.

(2) Randomly generate initial values of chaotic variables.

(3) Substitute Eq. (6) to iterate and update the number of iterations.

(4) If the maximum iteration number is met, go to step (5). Otherwise, return to step (3).

(5) End of iteration. The hybrid sequence is obtained and remapped to the individuals.

3.2.2. Mutation, hybridization and competition strategies

Three different individuals are randomly selected from the population. One of them is selected as the individual to be mutated, and the other two individuals are combined with the individual to be mutated after the vector difference scaling operation. It is expressed as follows.

$$V_i(t+1) = X_{q1}(t) + F * [X_{q2}(t) - X_{q3}(t)] \tag{6}$$

where $q1$, $q2$ and $q3$ represent three different random positions.

A dynamic mutation operator F is introduced to balance the convergence speed and accuracy. Therefore, the population diversity is assured in the early iteration stage, and the optimal solution is achieved in the later iteration stage. The dynamic mutation operator F is expressed as follows.

$$\begin{cases} F = F_0 * 2^{\tau} \\ \tau = \exp(1 - \frac{M_{\max}}{1+M_{\max}-t}) \end{cases} \tag{7}$$

where F_0 is the mutation rate of the population.

The cross individual isobtained from the target individual and the mutant individual after the crossover strategy is performed, which is expressed as:

$$U_{i,j}(t+1) = \begin{cases} V_{i,j}(t+1) rand(0,1) \le CR \\ X_{i,j}(t) \text{otherwise} \end{cases} \tag{8}$$

where $CR \in [0.8, 1]$ is a random hybridization parameter.

The current target individual and the crossover individual are made to compete, and then the next-generation population individual becomes the one with the better fitness value, which is expressed as:

$$X_{i,j}(t+1) = \begin{cases} U_i, j(t+1) f[U_{i,j}(t+1)] \le f[X_{i,j}(t)] \\ X_{i,j}(t) \text{otherwise} \end{cases} \tag{9}$$

3.2.3. Lévy flight

The Lévy flight mechanism is added to enhance the ability to escape from a local minimum. The individual position updates based on Lévy flight, which is expressed as

$$\begin{cases} X_{i,j}(t+1) = X_{i,j}(t) + L \oplus L(\lambda) \\ L = 0.01 * [X_{i,j}(t) - X_b^t] \end{cases} \tag{10}$$

$$step = u/|v|^{1/\gamma} \tag{11}$$

$$\begin{cases} \sigma_u = \left\{ \frac{\Gamma(1+\gamma)*\sin(\pi\gamma/2)}{\gamma*\Gamma[(1+\gamma)/2]*2^{(\gamma-1)/2}} \right\} \\ \sigma_v = 1 \end{cases} \tag{12}$$

where $\oplus$ is the point multiplication operation. L is the step-length control coefficient. L (λ) is the Lévy flight path function based on the Mantegna algorithm. *step* is the random step. γ is a constant selected as 1.5. u and v are random values that obey a normal distribution. σ_u and σ_v are respective variances.

3.2.4. The performance process

The flowchart of ISSA is shown in Figure 2. Its process is carried out as follows.

(1) Determine the maximum number of iterations, population size, search space range, dimension, and the ratio of producers and scroungers.

(2) Initialize population position based on the Bernoulli chaotic mapping. Calculate the fitness values, and record the current individual positions and their corresponding fitness values.

(3) Execute mutation, hybridization and competition strategies, and calculate the current individual position and fitness value.

(4) Update the location of the producers and scroungers, and calculate the current individual location and fitness value.

(5) Determine and update the position, and then perform a Lévy flight.

(6) After each iteration is completed, the fitness value and the average fitness value in the population are recalculated to update the proportion of producers and scroungers.

(7) Update the optimal and worst individual positions in the new population individual. If the fitness value is better than the original value, the individual position is replaced. If the maximum number of iterations is reached, the optimal sparrow position and fitness value is output. Otherwise, return to step (2) to repeat the same procedure.

3.3. Evaluation of model performance test

The performance efficiency comparison using ISSA, sparrow search algorithm (SSA), particle swarm optimization (PSO), differential Evolution (DE), gray wolf optimizer (GWO), whale optimization algorithm (WOA) and harris hawk optimizer (HHO) is implemented [37–39]. The search population number (N) is set as 50, and the search maximum number (M) is set as 500.

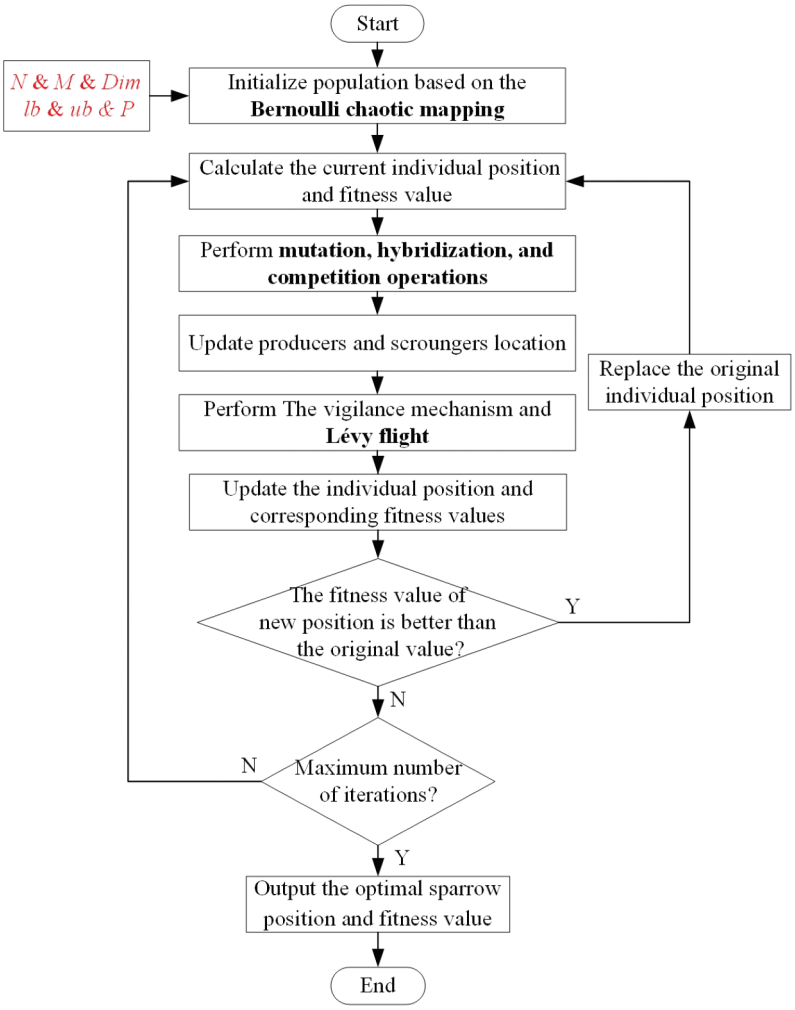

Figure 2. The flow chart of the ISSA.

Table 1. Algorithm parameters settings.

Algorithm	Parameters
PSO	c1 = c2 = 1.49; wmax = 0.9, wmin = 0.1
DE	F_0 = 0.5, CR = 0.9
GWO	A = 2a*rand(0, 1)-a, C = 2*rand(0, 1)
WOA	b = 1
HHO	E0 = 2*rand(0, 1)-1
SSA	P = 0.2, ST = 0.8
ISSA	F_0 = 0.5, CR = 0.5*[1+ rand(0, 1)], P = 0.2, ST = 0.8, p = 0.4, r_0 = 0.152

Detailed parameter settings are shown in Table 1. c1 and c2 are the learning coefficients in the PSO algorithm, wmax and wmin are the maximum and minimum weights. F_0 and CR are the mutation rate and hybridization parameter in DE algorithm. A and C are synergy coefficients in GWO algorithm, which decrease linearly from 2 to 0. b is the spiral coefficient in the WOA. E0 is the initial energy in the HHO algorithm. P and ST are the proportion of discoverers and the safety value in the SSA, respectively. In the ISSA, p and r_0 are initialization parameters of the chaotic mapping. In Table 2, there are 12 typical standard functions employed to verify the effectiveness of the ISSA [16,40]. The unimodal function has one global optimal solution, which is used to test the convergence speed and the local search ability. On the other hand, the multimodal function has multiple local optimal solutions, which are used to test the global search ability.

In the performance test, the minimum (Min), average (Avg) value and standard deviation (Std) values obtained from 30 times implementation are compared between all algorithms. The test results are shown in Table 3. According to the average value in Table 3, the results of all algorithms in each test function are compared and sorted. The last row in Table 3 is the average ranking result of each algorithm. When the average value is the same, the standard deviation is compared.

In the unimodal function, ISSA present the best results, compared with the PSO, DE, GWO and WOA. It indicates that the PSO and DE have worst optimization capability, showing large average and standard deviation values. In contrast, the ISSA has lower minimum,

Table 2. Standard test functions.

Function	Expression	Dim	F_{min}	Range
Unimodal	$F_1 = \sum_{j=1}^{d} x_j^2$	30	0	[−100, 100]
	$F_2 = \prod_{j=1}^{d} \lvert x_j \rvert + \sum_{j=1}^{d} \lvert x_j \rvert$	30	0	[−10, 10]
	$F_3 = \sum_{j=1}^{d} (\sum_{j=1}^{d} \lvert x_j \rvert)^2$	30	0	[−100, 100]
	$F_4 = \max_j \{\lvert x_j \rvert, 1 \le j \le d\}$	30	0	[−100, 100]
	$F_5 = \sum_{j=1}^{d} [100(x_{j+1} - x_j^2)^2 + (x_j - 1)^2]$	30	0	[−30,30]
	$F_6 = \sum_{j=1}^{d} ([x_j + 0.5])^2$	30	0	[−100, 100]
	$F_7 = \sum_{j=1}^{d} jx_j^4 + random[0, 1)$	30	0	[−1.28, 1.28]
Multimodal	$F_8 = \sum_{j=1}^{d} (x_j^2 - 10 * cos(2\pi x_j) + 10)$	30	0	[−5.12, 5.12]
	$F_9 = -20 * \exp(-0.2 * \sqrt{\frac{1}{d}\sum_{j=1}^{d} x_j^2})) - exp(\frac{1}{d}\sum_{j=1}^{d} cos(2\pi x_j)) + 20 + e$	30	0	[−32, 32]
	$F_{10} = \sum_{j=1}^{d} \frac{x_j^2}{4000} - \prod_{j=1}^{d} \cos(\frac{x_j}{\sqrt{j}}) + 1$	30	0	[−600, 600]
	$F_{11} = \frac{\pi}{n}\{10sin(\pi y_1) + \sum_{j=1}^{d-1} (y_j - 1)^2[1 + 10sin^2(\pi y_j + 1)] + (y_d + 1)^2\} + \sum_{j=1}^{d} u(x_j, 10, 100, 4)$ $y_j = 1 + \frac{x_j + 1}{4}, u(x_j, a, k, m) = \begin{cases} k(x_j - a)^m, x_j > a \\ 0, -a < x_j < a \\ k(-x_j - a)^m, x_j < -a \end{cases}$	30	0	[−50, 50]
	$F_{12} = 0.1\left\{\sin^2(3\pi x_1) + \sum_{j=1}^{d} (x_j - 1)^2 \begin{bmatrix} 1 + \sin^2(3\pi x_j + 1) \\ +(x_d - 1)^2[1 + \sin^2(2\pi x_d)] \end{bmatrix}\right\} + \sum_{j=1}^{d} u(x_j, 5, 100, 4)$	30	0	[−50, 50]

average and standard deviation values than GWO, WOA and HHO. It is found that only SSA and ISSA achieve the optimal value, i.e. 0, in F_1-F_4 function. Particularly, the optimization ability of the ISSA in the unimodal function is an order of magnitude higher than other algorithms. However, the ISSA performs poorly in F_7 function.

In the multimodal function, the GWO, WOA, HHO, SSA and ISSA can find the best value in both F_8 and F_{10} functions. The ISSA can find the better value in F_{11} function, and its overall average and standard deviation results are superior than others. In F_{12} function, the results from the ISSA are superior to other algorithms except the SSA.

4. The active distribution network with multi-microgrid system

4.1. The structure of the active distribution network with multi-microgrid system

he ADN model with MMG system is constructed as shown in Figure 3, which is divided into the MMG system layer and the ADN layer. It is managed by the Energy Decision Center (EDC) of the distribution network and the Energy Management Center (EMS) of each microgrid.

The MMG system considered in this study includes three independent microgrids, and there is no power transaction between each other. The lower-level MMG system is mainly composed of wind power generation system (WT), photovoltaic power generation system (PV), diesel engines (DIE), batteries (BAT), related inverters, controllers and user loads [41]. MG1 contains WT, MG2 contains PV, and MG3 contains both WT and PV.

Each microgrid combined wind or photovoltaic needs to reasonably configure the internal distributed power capacity and output, coordinate the power exchange with the upper distribution network, and reduce the cost while meeting the electrical load demand. The upper-level ADN contains power generator units. According to the electric power demand of the lower system and the demand of independent loads in the distribution network, a power generation plan is formulated to meet various needs while coordinating the optimal output of each unit.

4.1.1. Wind power generation system

The output of the wind power generation system is closely related to the wind speed, and the wind speed is easily affected by environmental factors and has great randomness. The output model of the wind power system is expressed as follows.

$$P_{WT} = \begin{cases} 00 \le v < v_{in} \\ \frac{P_{WT}^N v^3 - P_{WT}^N v_{in}^3}{v_N^3 - v_{in}^3} v_{in} \le v < v_N \\ P_{WT}^N v_N \le v < v_{out} \\ 0 v_{out} \le v \end{cases} \tag{13}$$

where P_{WT} is the output power of wind power. PN WT is the rated power. v, v_{in} and v_{out} are the rated wind speed, cut-in wind speed and cutout wind speed, respectively.

Table 3. Test results.

Function	Stats	PSO	DE	GWO	WOA	HHO	SSA	ISSA
F_1	Min	1.6569E-02	8.5201E-01	5.6481E-39	3.8667E-94	9.1182E-157	0.0000E+00	0.0000E+00
	Avg	7.6801E-02	1.9246E+00	1.2437E-33	5.9183E-85	3.8835E-116	2.3017E-146	**9.7291E-149**
	Std	4.0773E-02	7.3410E-01	1.9249E-33	2.4038E-84	1.4380E-115	1.2311E-145	5.3285E-148
	Rank	6	7	5	4	3	2	1
F_2	Min	9.5944E-01	1.5048E-02	4.4721E-23	3.3074E-60	1.0534E-79	0.0000E+00	0.0000E+00
	Avg	2.0744E+00	2.2620E-02	4.8804E-20	1.8637E-54	7.6171E-56	9.8676E-67	**6.1445E-70**
	Std	5.3988E-01	4.8919E-03	5.9373E-20	5.2329E-54	2.9563E-55	5.4046E-66	3.3655E-69
	Rank	7	6	5	4	3	2	1
F_3	Min	3.3364E-01	1.2821E+00	8.0936E-12	5.3127E-06	5.5729E-112	0.0000E+00	0.0000E+00
	Avg	6.2620E-01	2.7081E+00	4.0671E-08	5.2195E+02	4.4708E-94	1.5355E-79	**3.0332E-96**
	Std	2.5455E-01	9.6754E-01	9.6918E-08	1.1736E+03	2.4408E-93	8.3275E-79	1.6547E-95
	Rank	5	6	4	7	2	3	1
F_4	Min	1.9323E-01	1.0363E-02	1.1828E-10	4.0463E-09	6.0682E-81	0.0000E+00	0.0000E+00
	Avg	3.1913E-01	1.7467E-02	3.2897E-06	2.2065E-01	2.5602E-69	9.5821E-72	**2.5134E-83**
	Std	5.3028E-02	3.4446E-03	1.1764E-05	6.8649E-01	1.1669E-68	5.2482E-71	1.0446E-82
	Rank	7	5	4	6	3	2	1
F_5	Min	3.1553E+01	8.0373E+01	1.1356E-01	7.3065E-02	2.7720E-11	5.2349E-08	4.6295E-10
	Avg	4.2094E+01	3.4253E+02	2.5748E+01	1.3815E+01	4.5239E-03	2.2941E-05	**6.8485E-06**
	Std	8.7117E+00	1.9229E+02	4.8812E+00	1.3861E+01	1.3095E-02	3.4534E-05	2.0009E-05
	Rank	6	7	5	4	3	2	1
F_6	Min	3.4979E-02	9.6260E-01	3.5248E-05	3.5683E-08	3.8769E-12	8.6448E-15	2.1991E-16
	Avg	1.3849E-01	2.2277E+00	4.2465E-01	2.4953E-02	1.0829E-05	2.1560E-11	**1.0975E-11**
	Std	6.1884E-02	9.3911E-01	3.2170E-01	3.9624E-02	2.4786E-05	4.9167E-11	3.5317E-11
	Rank	6	7	5	4	3	2	1
F_7	Min	1.2080E-01	1.1948E-04	3.0793E-04	2.4731E-05	5.5699E-06	3.1102E-05	2.0904E-05
	Avg	1.0785E+00	2.6369E-04	9.3291E-04	8.7598E-04	**8.8957E-05**	5.4489E-04	6.3096E-04
	Std	1.2132E+00	1.1981E-04	4.7178E-04	1.0840E-03	1.3149E-04	5.3399E-04	5.9645E-04
	Rank	7	2	6	5	1	3	4
F_8	Min	2.1749E+01	1.7778E-01	0.0000E+00	0.0000E+00	0.0000E+00	0.0000E+00	0.0000E+00
	Avg	3.5393E+01	2.1179E-01	1.3217E+01	1.8948E-15	**0.0000E+00**	**0.0000E+00**	**0.0000E+00**
	Std	1.0977E+01	1.7282E-02	4.1813E+01	1.0378E-14	0.0000E+00	0.0000E+00	0.0000E+00
	Rank	7	6	5	4	1	1	1
F_9	Min	1.4926E-01	7.2524E-03	3.2863E-14	8.8818E-16	8.8818E-16	8.8818E-16	8.8818E-16
	Avg	8.8982E-01	9.5177E-03	6.6685E-01	4.6777E-15	**8.8818E-16**	**8.8818E-16**	**8.8818E-16**
	Std	4.8287E-01	1.0623E-03	3.6525E+00	2.6279E-15	0.0000E+00	0.0000E+00	0.0000E+00
	Rank	7	5	6	4	1	1	1
F_{10}	Min	1.1651E-03	8.2348E-03	0.0000E+00	0.0000E+00	0.0000E+00	0.0000E+00	0.0000E+00
	Avg	5.9972E-03	1.8545E-02	2.5907E-03	**0.0000E+00**	**0.0000E+00**	**0.0000E+00**	**0.0000E+00**
	Std	3.0646E-03	6.9387E-03	6.5483E-03	0.0000E+00	0.0000E+00	0.0000E+00	0.0000E+00
	Rank	6	7	5	1	1	1	1
F_{11}	Min	2.8620E-03	4.0943E-03	6.5932E-03	2.7018E-08	1.9336E-15	1.6271E-15	3.8925E-17
	Avg	1.4022E-02	9.0381E-03	5.6412E-01	1.6170E-03	1.1672E-06	3.3048E-12	**8.7533E-13**
	Std	9.1045E-03	3.6374E-03	2.3485E-03	2.9384E-09	3.9327E-06	9.6184E-12	3.4793E-12
	Rank	6	5	7	4	3	2	1
F_{12}	Min	6.6589E-02	2.9500E-02	8.0311E-05	5.5972E-09	1.9565E-11	2.2883E-15	1.0901E-14
	Avg	3.1852E-01	4.5673E+01	3.0377E-01	2.9185E-02	6.2954E-06	9.4817E-11	**4.2519E-11**
	Std	2.5665E-01	9.6892E+01	1.7311E-01	6.0898E-02	1.4203E-05	3.3902E-10	1.1277E-10
	Rank	6	7	5	4	3	2	1
Mean rank		6.31	5.92	5.15	4.08	2.15	2.00	1.46

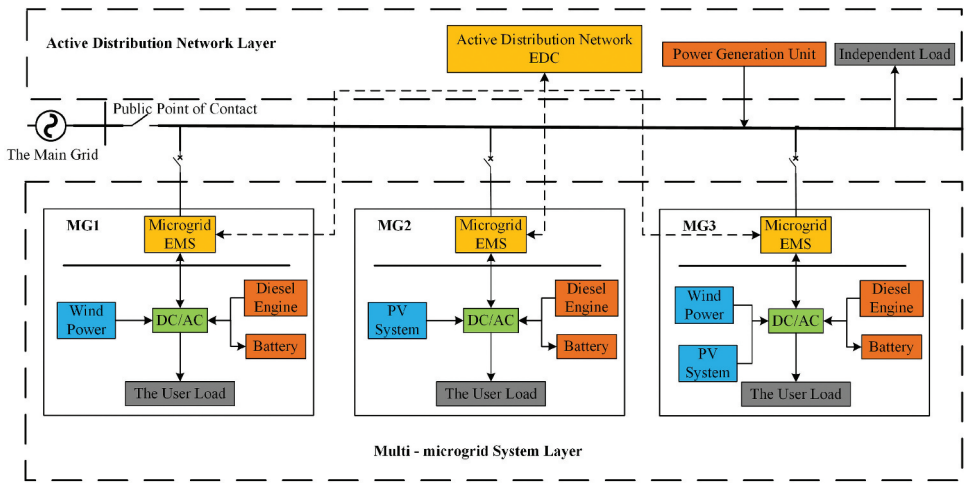

Figure 3. Hierarchical structure model of ADN with MMG system.

4.1.2. Photovoltaic power generation model

Generally, the output power of the photovoltaic power generation system is affected by a variety of environmental factors, among which the ambient temperature and light intensity are key factors in the output of photovoltaic power generation systems. The simplified output power model is given as follows.

$$\begin{cases} P_{PV} = P_{STC} G_C [1 + k(T_C - T_{STC})]/G_{STC} \\ T_C = T_t + 30 * G_C/1000 \end{cases} \quad (14)$$

where P_{PV} is the output power of photovoltaic power generation system. P_{STC} is the standard rated output power of the photovoltaic power generation system. T_t is the ambient temperature in the current environment. k is the power temperature coefficient. T_{STC} and G_{STC} are the standard ambient temperature and light intensity, respectively. Under the standard condition, T_{STC} and G_{STC} are 25℃ and 1000 W/m^2, respectively. T_C and G_C are the temperature and light intensity of the photovoltaic panel in the current environment, respectively.

4.1.3. Diesel engine model

The output power of diesel engines has a certain restriction range, which should not be lower than the minimum operating power. The relationship between the actual output power of the diesel engine and the consumption of fuel is shown as follows.

$$F_{DIE} = \alpha_1 P^N_{DIE} + \alpha_2 P_{DIE} \quad (15)$$

where F_{DIE} is the fuel consumption. PN DIE is the rated output power of the diesel engine. P_{DIE} is the output power. α_1 and α_2 are constants.

4.1.4. Energy storage system model

The capacity of the battery fluctuates in a small range as the surrounding temperature changes. According to the different operating status, the battery is divided into charging state, discharging state and static state. The battery energy storage system is expressed as follows.

$$\begin{cases} E_{BAT,C}(t) = (1-\eta)E_{BAT,C}(t-1) + P_c(t)\Delta t\eta_c/E_c(t) \\ E_{BAT,D}(t) = (1-\eta)E_{BAT,D}(t-1) - P_d(t)\Delta t/E_c(t)\eta_d \\ E_c(t) = E_{STC}[1 + \delta_b(T(t) - T_{STC})] \end{cases} \quad (16)$$

where $E_{BAT,C}(t\text{-}1)$ and $E_{BAT,D}(t\text{-}1)$ are the remaining power in the battery charging and discharging states at time t-1, respectively. $E_{BAT,C}(t)$ and $E_{BAT,D}(t)$ are the remaining power in the battery charging and discharging states at time t, respectively. E_{STC} and T_{STC} are the battery capacity and ambient temperature under standard conditions, respectively. $E_c(t)$ is the actual capacity of the battery. $P_c(t)$ and $P_d(t)$ are the charge and discharge power of the battery, respectively. η_c and η_d are the charge and discharge efficiency of the battery, respectively. $T(t)$ is the ambient temperature. η is the self-loss coefficient of the battery. δ_b is the capacity temperature coefficient of the battery. Δt is the time interval.

4.2. Hierarchical energy optimization management model

In the hierarchical energy optimization management, it is necessary to determine the management mode of the ADN with the internal MMG system. The distribution network EDC and the microgrid EMS are coordinated and controlled, and the entire ADN is globally optimized under the conditions of stable operation of the MMG system. It achieves the purpose of making full use of clean energy and peak-shaving and valley-filling in the system, and reduces the energy demand of the entire ADN on the main grid.

4.2.1. Multi-microgrid system layer

The MMG system layer includes three independent microgrids. The internal wind power generation system, photovoltaic power generation system, diesel engines, batteries and user load are controlled by microgrid EMS as the lower layer of hierarchical optimization management. Besides, power interaction with the ADN is required.

Each independent microgrid of the MMG system layer takes the lowest economic cost (g_1) and environmental cost (g_2) as the objective function, and takes the installed quantity and rated capacity of wind power generation system, photovoltaic power generation system, diesel engines and batteries as the decision variable X of the lower model.

(1) Economic objective function

The economic objective function (g_1) includes C_{Fuel} (fuel consumption cost), C_M (facility installation investment cost, operation and maintenance cost, replacement cost), C_T (cost for interacting with the grid), and C_P (energy penalty cost). C_M needs to be converted into daily value according to the discount rate and life cycle of the equipment, including the initial investment cost, the subsequent maintenance cost and the replacement cost. It is expressed as follows.

$$\min g_1 = C_{Fuel} + C_M + C_T + C_P \quad (17)$$

$$\mu(r,l) = r * (1+r)^l/[(1+r)^l - 1] \quad (18)$$

$$\begin{cases} C_{Fuel} = c_f \sum_{t=1}^{T} F_{DIE}(t) \\ C_M = \mu(r,l) \sum_{m=1}^{N_{DG}} [(c^I_m + c^M_m + c^R_m) N_m P^N_m/365l] \\ C_T = \sum_{t=1}^{T} [c_{buy}(t)P_{buy}(t) - c_{sell}(t)P_{sell}(t)] \\ C_P = \xi \sum_{t=1}^{T} [P_v(t) + P_w(t)] \end{cases} \quad (19)$$

where N_{DG} is the type of equipment, m = 1,2,3,4. c_f is the fuel price. $\mu(r,l)$ is the system depreciation coefficient. r is the discount rate of the equipment. l is the life cycle of the equipment. cI d, cM d and cR d are the investment, operation and maintenance and replacement costs of

the m-th equipment, respectively. $P_{buy}(t)$ and $P_{sell}(t)$ are the power purchased and sold by MMG system to the ADN at time t. $c_{buy}(t)$ and $c_{sell}(t)$ are the unit price of electricity purchased and sold by MMG system to the ADN at time t. $P_v(t)$ and $P_w(t)$ are the short and wasted parts of electric power. ξ is the penalty coefficient.

(2) Environmental objective function

Clean energy does not produce pollutants such as carbides, sulfides and nitrides, while diesel engines produce a certain amount of pollutants. Also, the electricity purchased by the MMG from the ADN produces pollutants. Therefore, the cost of treating these pollutants determines the environmental objective function (g_2), which is expressed as follows.

$$\min g_2 = \sum_{t=1}^{T}\sum_{k=1}^{K} c_k[\chi_{DIEk}P_{DIE}(t) + \chi_{gridk}P_{buy}(t)] \quad (20)$$

where $K \in \{CO_x, SO_x, NO_x\}$ is the type of pollutant, k = 1,2,3. c_k is the cost of the MMG system to treat each gram of the k-th pollutant. χ_{DIEk} is the emission coefficient of diesel engines to the k-th pollutant. χ_{gridk} is the emission coefficient of the k-th pollutant when the MMG system purchases electricity from the ADN.

(3) System constraints

The constraints in the MMG system include load balance constraints, energy storage system capacity constraints, equipment output constraints, and transaction constraints with the ADN.

Load balance needs to meet the load balance constraints. The output electric power of each microsource in the MMG is the same as the electric load demand.

$$\begin{aligned} &P_{WT}(t) + P_{PV}(t) + P_d(t) + P_{DIE}(t) + P_{buy}(t) \\ &\quad = P_{ULoad}(t) + P_c(t) + P_{sell}(t) \end{aligned} \quad (21)$$

where P_{ULoad} is the user load in the MMG system.

The expression of the battery constraints and the facility output constraints are given as follows.

$$\begin{cases} E_{BAT}^{min} \le E_{BAT}(t) \le E_{BAT}^{max} \\ P_c^{min} \le P_c(t) \le P_c^{max} \\ P_d^{min} \le P_d(t) \le P_d^{max} \\ P_{DIE}^{min} \le P_{DIE}(t) \le P_{DIE}^{max} \end{cases} \quad (22)$$

where P_c^{min} and P_c^{max} are the minimum and maximum charging power of the battery, respectively. P_d^{min} and P_d^{max} are the minimum and maximum discharge power of the battery, respectively. are given as follows. E_{BAT}^{min} and E_{BAT}^{max} are the minimum and maximum storage capacity of the battery, respectively. P_{DIE}^{min} is the minimum output power of diesel engines. On the contrary, P_{DIE}^{max} is the maximum output power of diesel engines. The trading constraints with the ADN are given as follows.

$$\begin{cases} P_{buy}^{min} \le P_{buy}(t) \le P_{buy}^{max} \\ P_{sell}^{min} \le P_{sell}(t) \le P_{sell}^{max} \end{cases} \quad (23)$$

where P_{buy}^{min} and P_{buy}^{max} are the minimum and maximum power purchases for the MMG system, respectively. P_{sell}^{min} and P_{sell}^{max} are the minimum and maximum electricity sales, respectively.

(4) Decision variable

Wind power generation system and photovoltaic power generation system are important sources of renewable energy. Their capacity determines the output of clean energy in the MMG system. However, excessive capacity leads to excessively high costs. The battery acts as an energy buffer in the MMG system through charging and discharging. If the capacity configuration is too low, the stored energy is not enough to meet the load demand, which will cause a shortage of load demand. The capacity configuration is large and causes power waste. Diesel engine is used as a backup power source, and its capacity configuration must be reasonable to ensure the reliable power supply of the system.

The quantity and installed capacity of the above four types of equipment are selected as the decision variable X of the system model.

$$X = [N_{WT}, N_{PV}, N_{DIE}, N_{BAT}, P_{WT}, P_{PV}, P_{DIE}, P_{BAT}] \quad (24)$$

where N_{WT}, N_{PV}, N_{DIE} and N_{BAT} are the number of wind power generation system, photovoltaic power generation system, diesel engines and batteries, respectively. P_{WT}, P_{PV}, P_{DIE} and P_{BAT} are the capacity of four devices, respectively.

4.2.2. Active distribution network layer

Each microgrid EMS sends the power interaction information of the lower system to the distribution network EDC. As the upper layer of hierarchical optimization management, ADN layer realizes the decision-making and management of the energy flow within the network.

The ADN layer takes the lowest operating cost of the power generation units (g_3) as the objective function, and uses the output ratio between the units as decision variable of the upper-level model. Unit One (PG1) undertakes the main power generation task and has a minimum proportion of 0.3, while the remaining units have a minimum proportion of 0.05. The output of each power generation unit is within the range. At the same time, the independent load power shortage rate (f_{LPSP}) is used as the evaluation index.

$$\min g_3 = \sum_{t=1}^{T}\sum_{j=1}^{N_G} [a_j P_{G,j}^2(t) + b_j P_{G,j}(t) + c_j] \quad (25)$$

$$f_{LPSP} = \sum_{t=1}^{T} [P_v(t)/P_{lLoad}(t)] \quad (26)$$

where N_G is the number of units. $P_{G,j}(t)$ is the output power of the j-th unit. a_j, b_j and c_j are operating parameters. $P_{lLoad}[t)$ is the independent load in the ADN.

4.3. System adaptive weight coefficients

42,proposed an adaptive dynamic weight factor model that used the objective function to measure economic cost and environmental cost. At each optimization cycle, the economic objective function (g_1] and the environmental objective function (g_2) are subjected to per-unit calculation to obtain $G_1(t)$ and $G_2(t)$, where the adaptive weight coefficients ω_1 and ω_2 are constructed. The comprehensive objective function F is defined as follows.

$$\begin{cases} \min g = \sum_{t=1}^{T} [\omega_1 G_1(t) + \omega_2 G_2(t)] \\ \omega_1 + \omega_2 = 1, \ \omega_1 = n_1 + n_2 G_1(t) \end{cases} \quad (27)$$

where $G_1(t)$ represents the unit value of the economic objective function (g_1) at time t. n_1 and n_2 are linear correlation coefficients, and the sum of ω_1 and ω_2 is a constant, i.e. 1. In the process of algorithm optimization, the ω_1 and ω_2 are dynamically selected. When G_1 decreases, ω_1 decreases correspondingly. Meanwhile, ω_2 increases, and the proportion of environmental cost optimization increases. When G_1 increases, ω_1 increases correspondingly, where the economic cost is regarded as a relatively large proportion.

4.4. The operation strategy of the hierarchical energy optimization management model

In the traditional operation strategy, the MMG system preferentially consumes the electric power generated by wind power generation system and photovoltaic power generation system. When the output of renewable energy is insufficient, the remaining load demand has two compensation methods. The first method is provided by battery discharge first, and then purchase electricity from the upper-level distribution network. The second method is to purchase electricity from the upper-level distribution network first, and then discharge from the battery. When there is a surplus of renewable energy output, there are also two methods to deal with the surplus power. The first method is to charge the battery first, and then sell electricity to the upper-level distribution network. The second method is to sell electricity to the upper-level distribution network first, and then charge the battery.

Long-term charging and discharging of the battery affect its life, and the power interaction with the upper distribution network affect the economic cost of the lower microgrid. Therefore, a MMG operation strategy that mixes the battery and the power interaction is designed. By calculating the unbalanced power when the wind and solar output exceeds or is less than the load demand at a certain time, the proportion of the "storage-network" configuration proportion is used as an optimization variable to find the optimal ratio. The flow of the specific operation strategy of the hierarchical energy optimization management model is shown in Figure 4.

5. Performance results and discussions

5.1. Model test environments

Two typical days in spring and summer are selected to represent the load demand of the MMG system under different conditions throughout the year. The data of user load in microgrid and independent load in ADN is collected from New York Independent System Operator (NYISO), as shown in Figure 5.

In addition, two typical days weather conditions are shown in Figure 6. The corresponding local meteorological data, such as wind speed, temperature and light intensity, used the Meteonorm 7 within 24 hours period. Each independent microgrid is in the same area, so the environmental factors that affect the output of wind and photovoltaic power at the MMG system layer are the same.

The entire tests were performed using MATLAB R2016a software under Microsoft Windows 10 operating system. The computer configuration is described as: Core i5-5200 U, 2.20 GHz, 4 GB RAM. The summer day has higher temperature and light intensity than the spring day, which causes more photovoltaic system output. In addition, the spring day has higher wind speed than the summer day, which causes more wind power system output.

The parameters of each power generation unit in the ADN layer refer to 43, as shown in Table 4. PG3 only runs on the summer day. The specifications of the facilities used in the MMG are shown in Table 5 [41]. The maximum remaining capacity in the battery are set as 90% in the rated capacity. The maximum output of the battery is 0.75 of the maximum capacity.

Besides, the facilities depreciation coefficient is assumed as 0.08. The unit prices of each pollutant treatment and the pollutant emission amount [g/kWh) in CO_x, NO_x, and SO_x refer to 44, as shown in Table 6. Time-of-use price of electricity interacting with the main grid refers to 45, as shown in Table 7. The price of diesel is 6.11 RMB/L. Note that 1 RMB $\approx$ 0.15 USD.

5.2. System operation optimization analysis using ISSA

In this part, the system operation optimization analysis is carried out based on the model proposed in the Section 4. Chapter 5.2.1 is the ADN layer, and Section 5.2.2 is the MMG system layer. The system operation strategy is the improvement strategy proposed in the Section 4.4, and the model solution method is ISSA proposed in the Section 3.

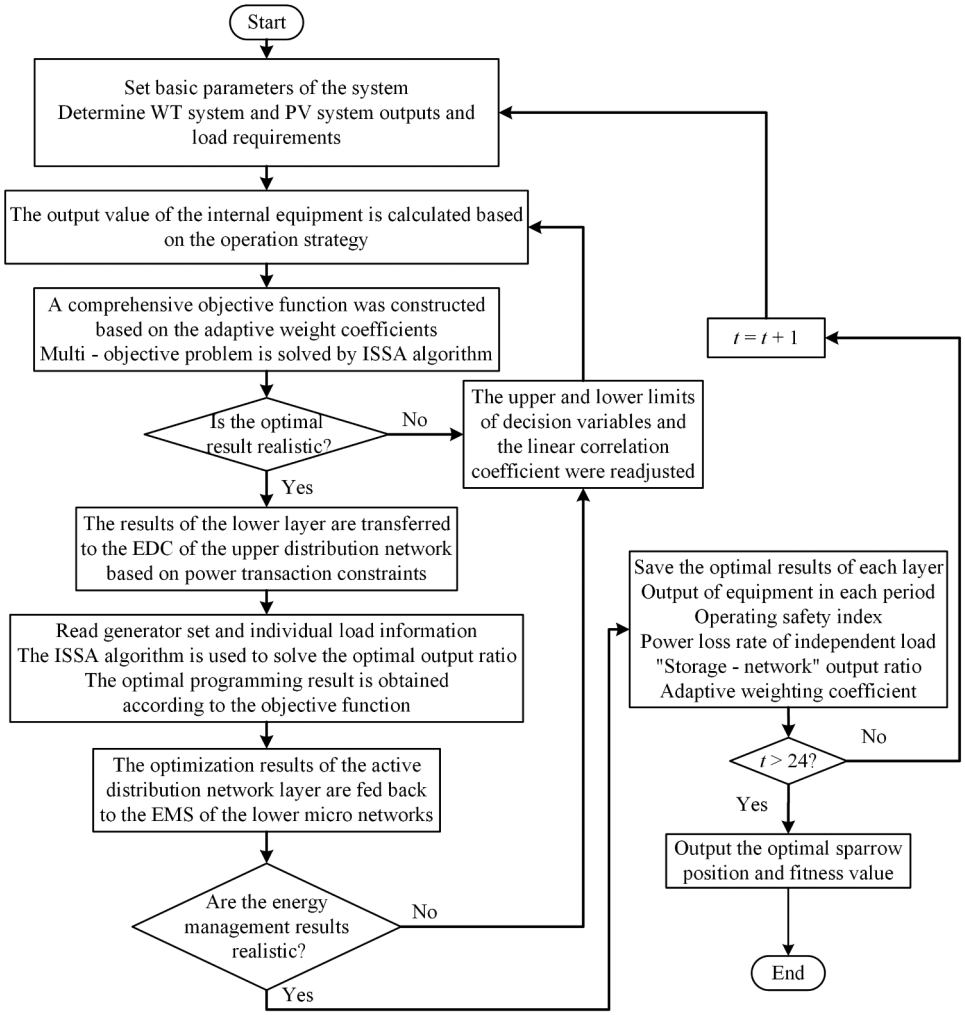

Figure 4. The operational strategy flowchart of hierarchical optimization model.

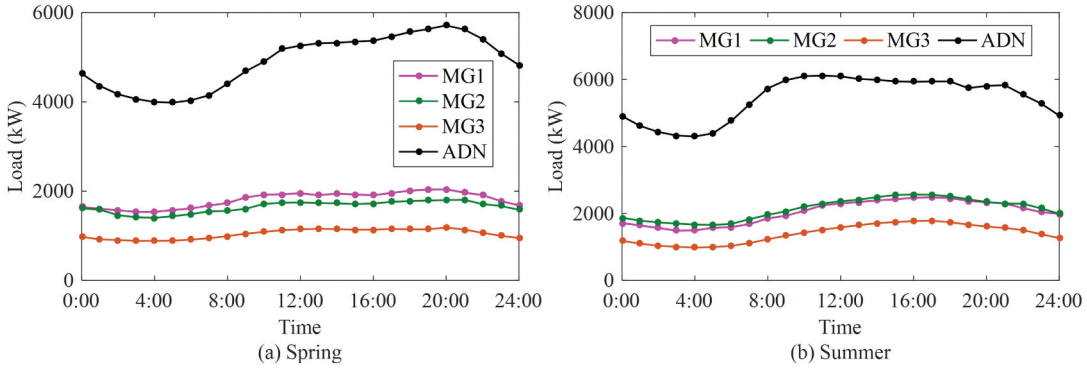

Figure 5. The load demand curves of two typical days.

5.2.1. Active distribution network layer

The power generation units' output of the ADN in two typical days and the power transactions with each microgrid are shown in Figure 7 and 8.

Figure 7, the overall output of each power generation unit changes with the fluctuation of the independent load. PG1 is the main power generation unit, and there is no unit saturation. Due to the electric load balance constraint in the ADN, the power transaction of the MMG system to the ADN is in the state of selling electricity, during the period of 8:00–11:00 and 14:00–16:00 in the spring day, and the output of each unit showed a downward trend. During the time period of 8:00–12:00 in the summer day, the output of each unit also showed a significant downward trend.

Figure 8 indicated during the time period of 1:00–7:00 and 21:00–24:00 in the spring day, the multi-micro grid system has a greater demand for power purchase

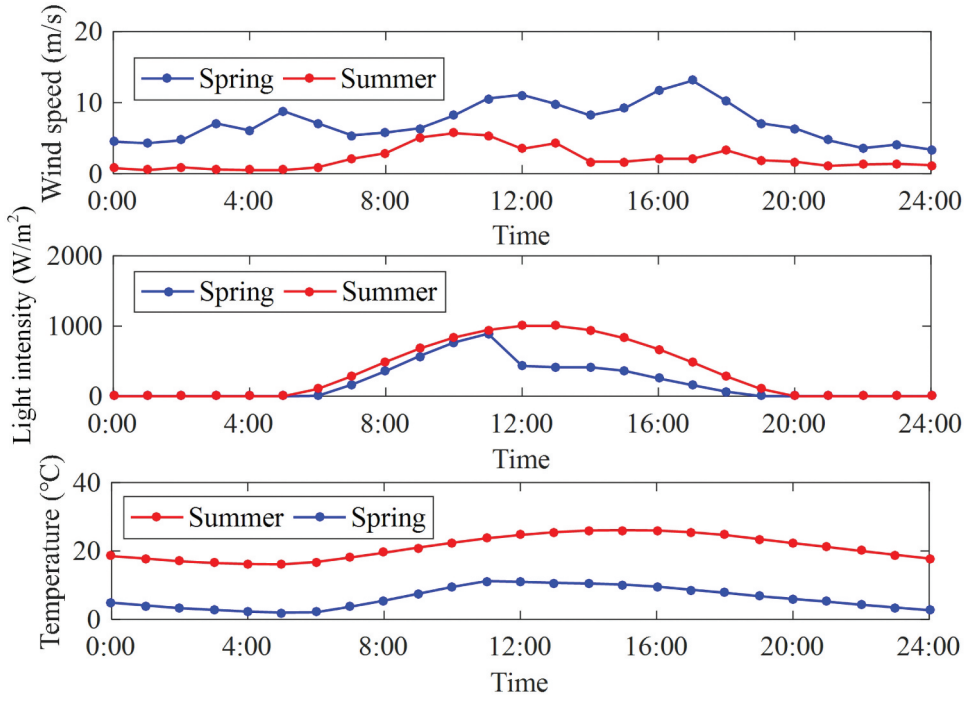

Figure 6. The weather conditions of two typical days.

Table 4. Parameters of each power generation unit.

Power generation unit	Lower output (kW)	Upper output (kW)	Operating parameters		
			a	*b*	*c*
PG1	200	3500	0.0004	0.25	40
PG2	100	2500	0.0006	0.20	30
PG3	300	1200	0.0450	6.00	15
PG4	100	1500	0.0360	5.00	18
PG5	100	1500	0.0280	3.75	18

Table 6. Pollutant emission amount (g/kWh).

Pollutant	Diesel engine	Main grid
CO_x	649	889
NO_x	9890	1.6
SO_x	0.206	1.8

Table 7. Time-of-use price of electricity interacting.

Period	Time	k_{buy} (RMB/kWh)	k_{sell} (RMB/kWh)
Peak	6:00–11:00, 19:00–23:00	1.21	1.02
Valley	23:00–6:00	0.43	0.27
Balance	11:00–19:00	0.69	0.50

from the ADN. Due to the large wind and solar output, the sales of electricity to the ADN are large at 9:00–13:00 and 16:00–18:00. During the time period of 1:00–6:00 and 18:00–24:00 in the summer day, due to the limited output of wind and solar, the power purchase demand of the MMG system from the ADN reaches the upper limit of power trading. Only in the period of 9:00–15:00, there are electricity sales to the ADN.

5.2.2. Multi-microgrid system layer

The operation of MG1 in two typical days is shown in Figure 9. In the spring day, the wind power generation system produces more power throughout the entire time period. During the period of 19:00–24:00, due to the low wind speed, it is necessary to discharge the battery or purchase electricity from the upper ADN. The diesel engine has almost no output. During the time period of 11:00–18:00, the battery charging and the sale of electricity to the upper ADN are relatively large. In the summer day, affected by the wind speed, the wind power generation system only produces much power during the time period of 9:00–13:00. At this time, the battery is charged and the electricity is sold to the upper ADN. During the rest of the time period, the power purchases from the upper-level ADN

Table 5. Facilities specifications.

Facilities	Maximum capacity (kW)	Investment cost (RMB/kW)	Operation and maintenance cost (RMB/kW)	Replacement cost (RMB/kW)	Life (years)
Wind power	25	4535	35.4	0	20
Photovoltaic power	15	5000	88.7	0	25
Diesel engine	25	1283	25.7	1000	9
Battery	5	567	5.7	453	2.5

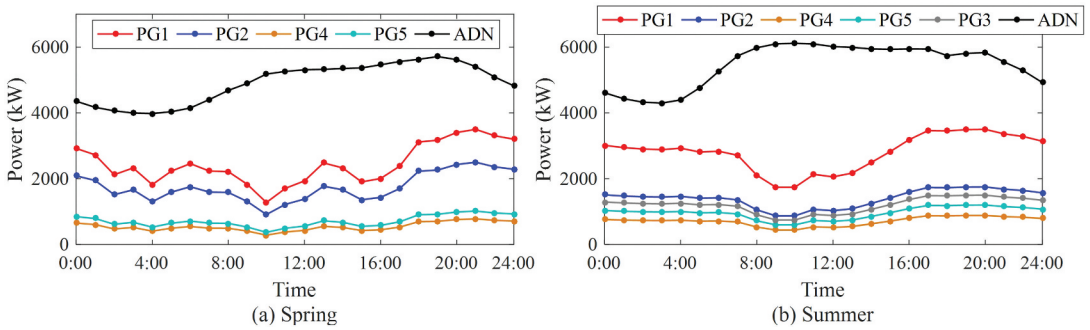

Figure 7. Two typical daily output curves of power generator units.

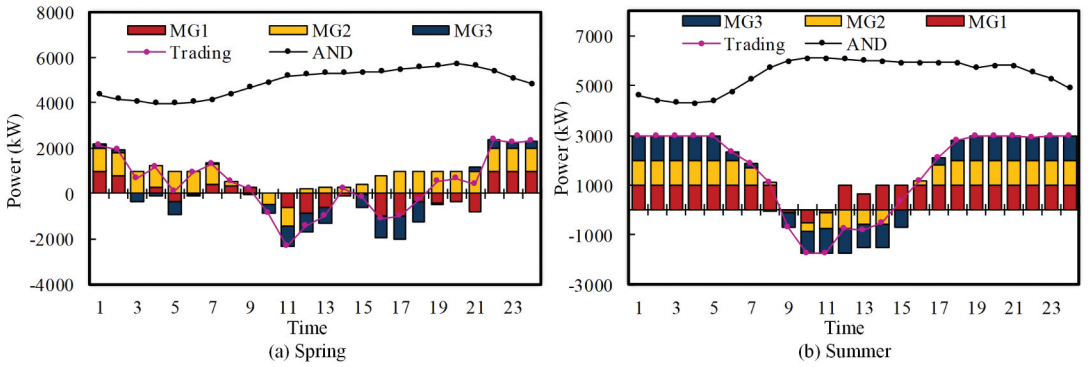

Figure 8. Power trading curves.

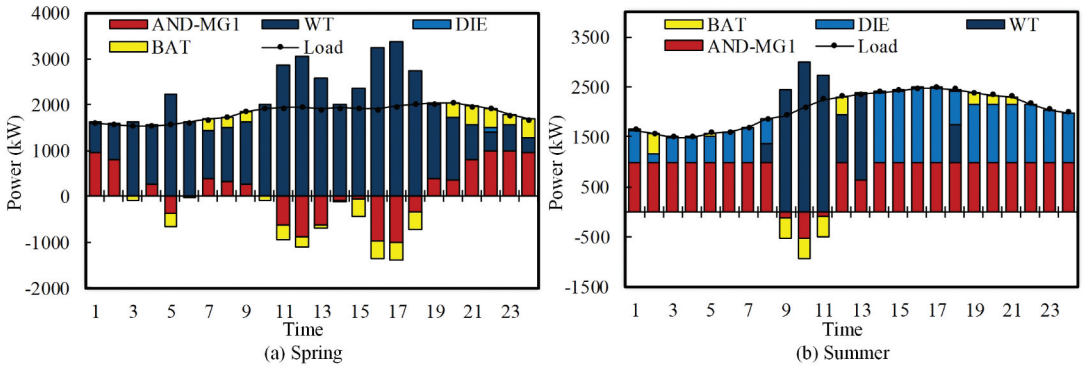

Figure 9. MG1 operation optimization results.

reached the peak value, and the diesel engine output was relatively large and made up for the power shortage.

The operation of MG2 in two typical days is shown in Figure 10. Affected by environmental factors, the photovoltaic power generation system has a large

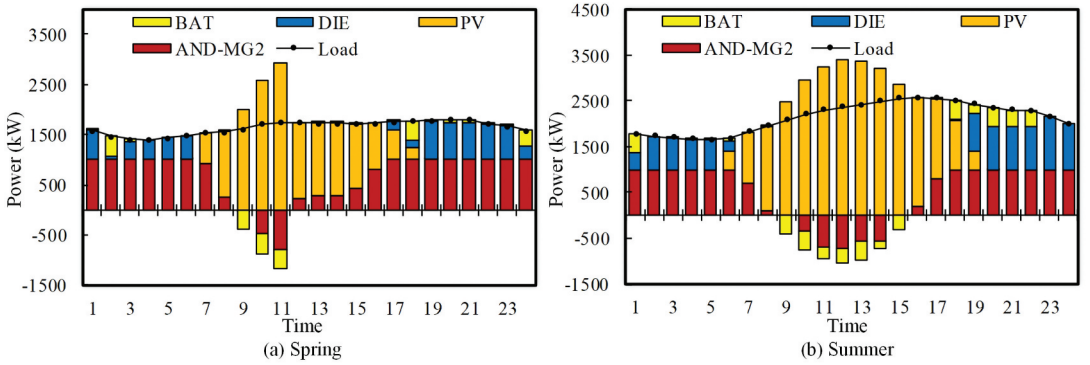

Figure 10. MG2 operation optimization results.

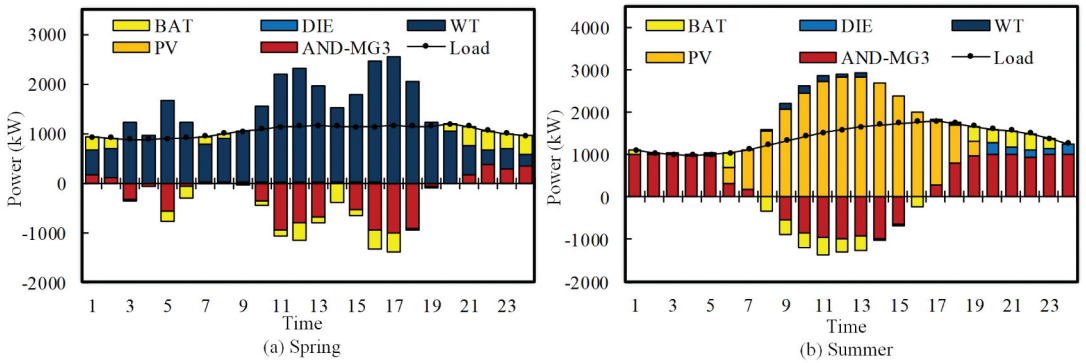

Figure 11. MG3 operation optimization results.

output during the time period of 8:00–16:00, and the power in summer is greater than the power in spring. During 9:00–11:00 in the spring day and 9:00–15:00 in the summer day, the battery is charged and power is sold to the upper ADN. In two typical days, the power purchase from the upper ADN and diesel engines will be greater during the time periods of 1:00–7:00 and 17:00–24:00.

The operation of MG3 in two typical days is shown in Figure 11. Since the MG3 includes wind power generation system and photovoltaic power generation system, wind resources are fully utilized in the spring day, and wind power is relatively large. While in the summer day, photovoltaic power is mainly relied on. In two typical days, the battery is replenished accordingly, and the MG3 sells more power to the upper ADN, resulting in a small output of the diesel engine during the whole time period.

5.3. Energy optimization management analysis in typical days

In the optimization model, the upper layer takes the lowest operating cost of the generator power unit as the optimization goal, and the lower layer takes the lowest economic cost and environmental cost as the optimization goal, which is finally expressed as the total cost of the entire system. The comparison results of two typical days are shown in Table 8.

The ISSA, SSA, WOA and GWO models are used to evaluate the optimization effectiveness of the hierarchical energy optimization management model using the parameter settings shown in Table 1. The comparison results in two typical days are concluded in Table 7, where C_1 and C_2 are obtained from Eq.(17), Eq.(21) and Eq.(25), respectively. Note that the value C_1 is the sum of g_1 and g_2 of the MMG system, which indicates the total cost of the economy and environment, and the value C_2 is the lowest operating cost of the power generation units (g_3). The value C is the sum of C_1 and C_2. which indicates the total cost of the entire system.

The value C using ISSA has a better optimization effect than others in two typical days. Both ISSA, SSA and GWO have similar results that are slightly better than WOA. It is clear that the overall optimization results of the ISSA are generally superior to SSA, WOA and GWO, which can effectively reduce the economic cost and environmental cost. In addition, the independent load power shortage rate (f_{LPSP}) is at a normal value, and the value f_{LPSP} of the ISSA is at the minimum.

The total economic and environmental costs in summer are higher than those in spring due to the large daily load demand in summer. Besides, renewable energy output in summer is less than the spring day, and the demand for electricity load in the summer day is large, which can increase the total cost.

The convergence curves of the four algorithms performance in two typical seasons are shown in Figure 12. The initial optimal value in the early stage of the iteration from the WOA is larger, and its convergence speed is slow. The convergence accuracy of the GWO, WOA and SSA is lower than ISSA. The convergence speed of the GWO and WOA is slower than SSA and ISSA. The ISSA achieves better convergence rate and result than others at the range of 50–100 iterations. In conclusion, it

Table 8. Comparison results of two typical days.

Typical days	Models	C_1/RMB	C_2/RMB	C/RMB	f_{LPSP}
Spring	GWO	4.5484×10^6	1.1293×10^6	5.6778×10^6	7.4435×10^{-4}
	WOA	1.2305×10^7	7.8856×10^5	1.3093×10^7	3.0481×10^{-3}
	SSA	4.6510×10^6	1.2046×10^6	$5,8556 \times 10^6$	4.7415×10^{-15}
	ISSA	4.3486×10^6	8.8824×10^5	5.2369×10^6	0
Summer	GWO	1.8390×10^7	1.6062×10^6	1.9996×10^7	1.4828×10^{-15}
	WOA	2.4972×10^7	1.6926×10^6	2.6665×10^7	6.6305×10^{-4}
	SSA	1.7262×10^7	1.6052×10^6	1.8867×10^7	1.2975×10^{-15}
	ISSA	1.6968×10^7	1.5935×10^6	1.8526×10^7	0

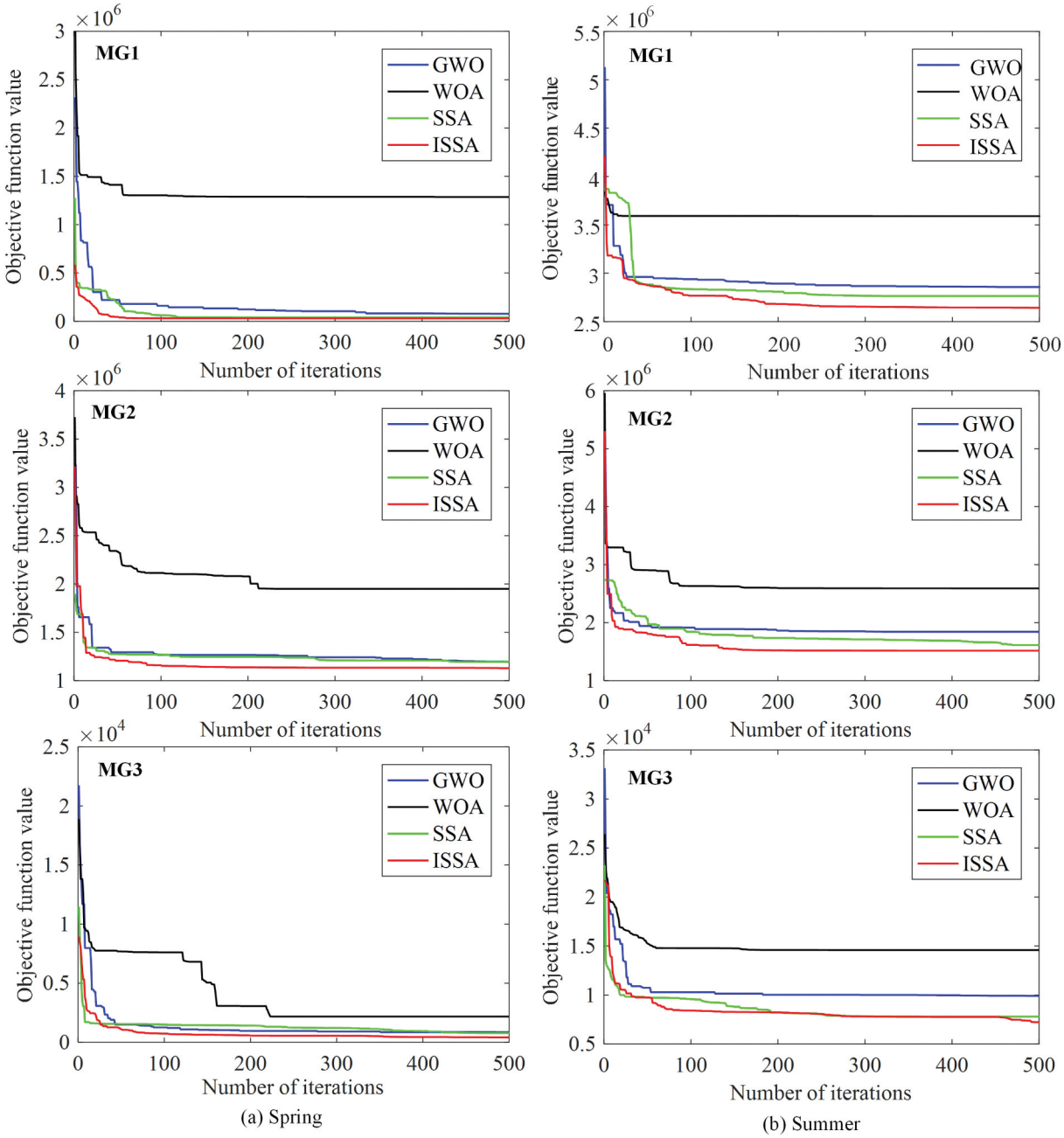

Figure 12. Convergence curves of the four algorithms in two typical days.

is obvious that the ISSA model is superior in terms of the convergence speed and convergence accuracy in the MMG system operation optimization.

5.4. Performance comparison of different control strategies

Using the ISSA, the improved operation strategy in Section 4.4 is compared with the two traditional strategies. The output sequence of Strategy I is WT-PV-BAT-AND-DIE, and the output sequence of Strategy II is WT-PV-AND-BAT-DIE. Strategy III is the improved operation strategy. The optimization results are shown in Table 9.

The total cost of the entire system (C) with Strategy I and Strategy II has higher cost than Strategy III. Compared with Strategy III, C using Strategy I increases 15.81% in the spring day. On the other hand, it increases 2.36% in the summer day. Compared with Strategy III, C using the Strategy II increases 28.75% in the spring day, and it increases 8.79% in the summer day. In addition, Strategy III can effectively reduce the independent load power shortage rate (f_{LPSP}).

In the Strategy III, the optimal result of the "storage-network" configuration proportion of the MMG is shown in Figure 13. The overall "storage-network" configuration proportion change trend is in line with the operational optimization results shown in.

Table 9. Comparison results of two typical days.

Typical days	Strategy	C_1/RMB	C_2/RMB	C/RMB	f_{LPSP}
Spring	I	5.1402×10^6	9.2468×10^5	6.0649×10^6	6.0822×10^{-7}
	II	5.6330×10^6	1.1093×10^6	6.7423×10^6	2.5583×10^{-7}
	III	4.3486×10^6	8.8824×10^5	5.2369×10^6	0
Summer	I	1.7435×10^7	1.5281×10^6	1.8963×10^7	1.1121×10^{-15}
	II	1.8631×10^7	1.5248×10^6	2.0155×10^7	1.4828×10^{-15}
	III	1.6968×10^7	1.5935×10^6	1.8526×10^7	0

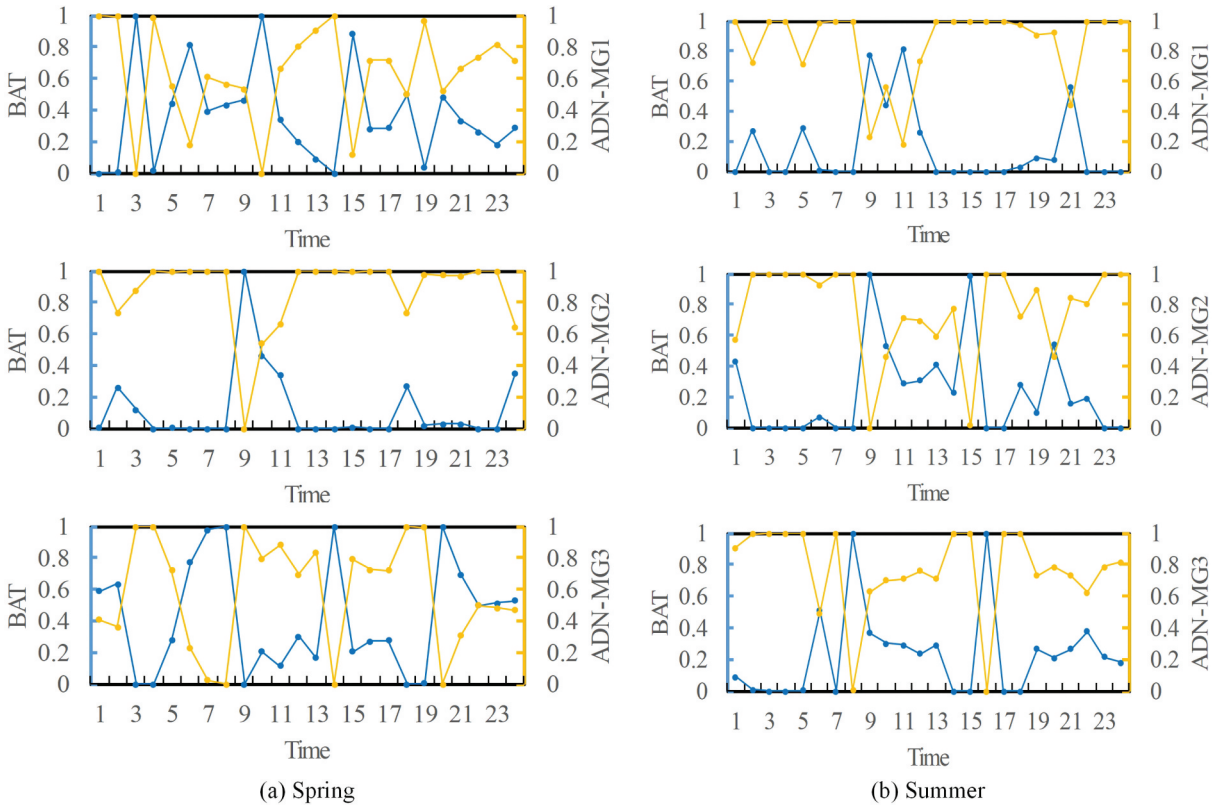

Figure 13. Optimization results of the "storage-network" configuration proportion.

In the spring day, the wind power generation system has a larger output, so the power interaction value is larger. The battery can provide part of the power after being charged, and it accounts for a relatively large amount at this time. In the summer day, the amount of power purchased from the upper ADN during the time periods of 1:00–8:00 and 17:00–24:00 is relatively large, and the proportion of power interaction is greater than the proportion of the battery. During the time period of 19:00–21:00, due to battery discharge and increased diesel engine output, the power interaction ratio decreases. During the time period of 9:00–14:00, the large amount of photovoltaic power generation promotes the decrease in electricity sales level and the increase in the battery charging, resulting in the fluctuation of "storage-network" configuration proportion.

5.5. Adaptive weight coefficients analysis in typical days

In the MMG system, the adaptive weight coefficients dynamically measure the economic objective function (g_1) and the environmental objective function (g_2) of each time period in the optimization cycle. The optimization results are shown in Figure 14. The change trend of the adaptive weight coefficients is in line with the operational optimization results shown in Figure 9.

In the spring day, for MG1, the environmental cost weight is greater in the time periods of 2:00–6:00 and 10:00–18:00, which are used to limit pollutant treatment costs. The economic cost weight increases in the time periods of 7:00–9:00 and 19:00–24:00 to limit the power interaction cost. In the summer day, due to the small output of the wind power generation system, the economic cost weight is greater than the environmental cost

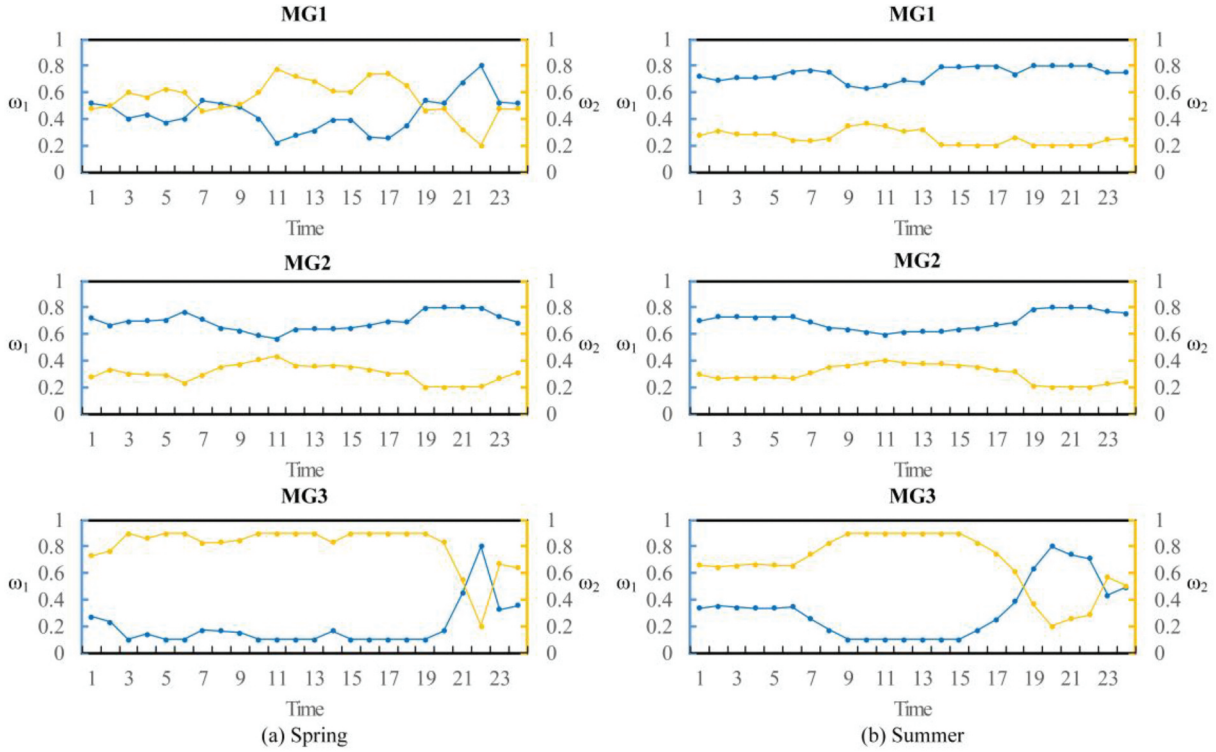

Figure 14. Optimization results of the adaptive weight coefficients.

weight in the whole time period, realizing the dynamic optimization of the economic objective function in the whole cycle.

For MG2, the output of photovoltaic power generation system is greatly affected by environmental factors. In the whole time period, the output of renewable energy is limited, and the power purchase from the upper ADN and the output of diesel engines increase, resulting in the economic cost weight is greater than the environmental cost weight.

For MG3, the environmental cost weight is greater in the time periods of 1:00–20:00 and 23:00–24:00. The economic cost weight increases in the time periods of 21:00–22:00. In the summer day, the environmental cost weight is greater in the time periods of 1:00–18:00 and 23:00–24:00. The economic cost weight increases in the time periods of 19:00–22:00.

6. Discussion

This study has a positive impact in industry, environment and society perspectives [46, 47]. The proposed ADN model with MMG system model can effectively reduce operating costs while ensuring the safety and stability of the system. The proposed ISSA can increase the utilization rate of renewable energy and reduce the emission of system pollutants while reducing economic costs. It has an important impact on the realization of environmental protection and the promotion of social benefits. Meanwhile, the ISSA could develop the global search capability of the original sparrow search algorithm, and the proposed ISSA is used in other fields to achieve optimal solutions.

This study proposes a hierarchical energy optimization management method for the ADN with MMG system, and its scientific novelty is as follows. (1) The ADN model with MMG system is divided into the MMG system layer and the ADN layer, and adaptive weight coefficients are used to transform the multi-objective problem into a single-objective problem under dynamic programming; (2) An ISSA is proposed by introducing the Bernoulli chaotic mapping, Lévy flight and the operations of mutation, crossover and competition; and (3) A MMG operation strategy is proposed for the sake of strengthening the power supply capacity of the system.

7. Concluding remarks

The energy used to support the MMG system may come from renewable energy sources, like wind power, solar power, etc. The ADN with MMG system is therefore under a big threat due to their fluctuating nature. The models and methods proposed are of great significance for the economic operation and environmental protection of MMG ADN, and the major conclusions are concluded as follows.

- The hierarchical energy optimization management of the ADN with MMG system can not only reduce the generating cost of power generator units at the ADN layer, but also reduce the economic and environmental costs of the MMG system layer.
- The multi-objective problem is transformed into a single-objective problem by introducing adaptive weight coefficients in the proposed model. Therefore, the control strategy and decision variables in the MMG operation is determined to achieve both economic cost and environmental cost more reasonably.
- The ISSA has presented better optimization ability in accuracy and convergence process than traditional methods. The GWO, WOA, SSA and ISSA are tested under two typical days such as spring and summer. The results verify that the ISSA presents the best power capacity configuration.
- The operation strategy for the interactive hybrid configuration of the battery and the power interaction can strengthen the "storage-network" joint output capability and effectively improve the system structure. The mixed configuration operation strategy improves the fixed output sequence mode of distributed power generation, and reduces the system cost under the same conditions compared with the traditional operation strategy [48–49].

This study only involves two types of renewable energy, namely wind energy and solar energy, which has certain limitations. In the future work, the multiple time scales, trading mechanism and more types of renewable energy are fully considered to further systematically establish the power operation scheduling model of MMG system.

Disclosure statement

No potential conflict of interest was reported by the author(s).

Funding

This work was supported by the Natural Science Foundation of Tianjin [19JCZDJC32100].

ORCID

Ming-Lang Tseng http://orcid.org/0000-0002-2702-3590

References

[1] Li LL, Zhao X, Tseng ML, et al. Short-term wind power forecasting based on support vector machine with improved dragonfly algorithm. J Clean Prod. 2020;242:118447.
[2] Wang SX, Zhang XY, Wu L, et al. New metrics for assessing the performance of multi-microgrid systems in stand-alone mode. Int J Electr Power Energy Syst. 2018;98:382–388.
[3] Xu YC, Zhang J, Wang P, et al. Research on the bi-level optimization model of distribution network based on distributed cooperative control. IEEE Access. 2021;9:11798–11810.
[4] Arefifar SA, Ordonez M, Mohamed YAI. Energy management in multi-microgrid systems—Development and Assessment. IEEE Trans Power Syst. 2017;32 (2):910–922.
[5] Mokryani G, Hu YF, Papadopoulos P, et al. Deterministic approach for active distribution networks planning with high penetration of wind and solar power. Renewable Energy. 2017;113:942–951.
[6] Chen CW, Chen WK, Chen CW, et al. An empirical study of willingness to renewable energy installation using importance-performance analysis: the case of Taiwan. J Ind Prod Eng. 2019;36(7):451–460.
[7] Luo YH, Nie QB, Yang DS, et al. Robust optimal operation of active distribution network based on minimum confidence interval of distributed energy beta distribution. J Mod Power Syst Clean Energy. 2021;9 (2):423–430.
[8] Zeng B, Wen JQ, Shi JY, et al. A multi-level approach to active distribution system planning for efficient renewable energy harvesting in a deregulated environment. Energy. 2016;96:614–624.
[9] Aghdam FH, Kalantari NT, Mohammadi-Ivatloo B. A stochastic optimal scheduling of multi-microgrid systems considering emissions: a chance constrained model. J Clean Prod. 2020;275:122965.
[10] Cong PW, Tang W, Zhang L, et al. Day-ahead active power scheduling in active distribution network considering renewable energy generation forecast errors. Energies. 2017;10(9):1291.
[11] Khavari F, Badri A, Zangeneh A. Energy management in multi-microgrids considering point of common coupling constraint. Int J Electr Power Energy Syst. 2020;115:105465.
[12] Xiang Y, Liu JY, Li FR, et al. Optimal active distribution network planning: a review. Electr Pow Compo Sys. 2016;44(10):1075–1094.
[13] Zubo RHA, Mokryani G. Active distribution network operation: a market-based approach. IEEE Syst J. 2020;14(1):1405.
[14] Tang Y, Liu Z, Li L. Performance comparison of a distributed energy system under different control strategies with a conventional energy system. Energies. 2019;12(24):4613.
[15] Li LL, Yang YF, Wang CH, et al. Biogeography-based optimization based on population competition strategy for solving the substation location problem. Expert Syst Appl. 2018;97:290–302.

[16] Xue J, Shen B. A novel swarm intelligence optimization approach: sparrow search algorithm. Syst Sci Contr Eng. 2020;8(1):22–34.
[17] Liu YW, Feng H, Li HY, et al. An improved whale algorithm for support vector machine prediction of photovoltaic power generation. Symmetry. 2021;13(2):212.
[18] Tian H, Wang KQ, Yu B, et al. Hybrid improved Sparrow Search Algorithm and sequential quadratic programming for solving the cost minimization of a hybrid photovoltaic, diesel generator, and battery energy storage system. Energy Sources Part A. 2021;1–17. DOI:10.1080/15567036.2021.1905111
[19] Cheng S, Su GC, Zhao LL, et al. Dynamic dispatch optimization of microgrid based on a QS-PSO algorithm. J Renewable Sustainable Energy. 2017;9 (4):045505.
[20] Karimi H, Bahmani R, Jadid S, et al. Dynamic transactive energy in multi-microgrid systems considering independence performance index: a multi-objective optimization framework. Int J Electr Power Energy Syst. 2021;126:106563.
[21] Sun YY, Cai ZX, Zhang ZY, et al. Coordinated energy scheduling of a distributed multi-microgrid system based on multi-agent decisions. Energies. 2020;13 (16):4077.
[22] Wu KM, Li Q, Chen ZY, et al. Distributed optimization method with weighted gradients for economic dispatch problem of multi-microgrid systems. Energy. 2021;222:119898.
[23] Liu ZH, Yi YQ, Yang JH, et al. Optimal planning and operation of dispatchable active power resources for islanded multi-microgrids under decentralised collaborative dispatch framework . IET Gener Transm Distrib. 2020;14(3):408–422.
[24] Wang LL, Zhu Z, Jiang CW, et al. Bi-level robust optimization for distribution system with multiple microgrids considering uncertainty distribution locational marginal price. IEEE Trans Smart Grid. 2021;12 (2):1104–1117.
[25] Funde N, Dhabu M, Deshpande P. CLOES: cross-layer optimal energy scheduling mechanism in a smart distributed multi-microgrid system. J Ambient Intell Humaniz Comput. 2020;11(11):4765–4783.
[26] Ge LJ, Song ZS, Xu XD, et al. Dynamic networking of islanded regional multi-microgrid networks based on graph theory and multi-objective evolutionary optimization. Int Trans Electr Energy Syst. 2020;31(1): e12687.
[27] Kong XY, Liu DH, Wang CS, et al. Optimal operation strategy for interconnected microgrids in market environment considering uncertainty. Appl Energy. 2020;275:115336.
[28] Jin SP, Wang SP, Fang F. Game theoretical analysis on capacity configuration for microgrid based on multi-agent system. Int J Electr Power Energy Syst. 2021;125:106485.
[29] Lainfiesta M, Zhang XW. Frequency stability and economic operation of transactive multi-microgrid systems with variable interconnection configurations. Energies. 2020;13(10):2485.
[30] Qiu HF, Gu W, Xu YL, et al. Robustly multi-microgrid scheduling: stakeholder-parallelizing distributed optimization. IEEE Trans Sustainable Energy. 2020;11 (2):988–1001.
[31] Ruan H, Gao HJ, Liu YB, et al. Distributed voltage control in active distribution network considering renewable energy: a novel network partitioning method. IEEE Trans Power Syst. 2020;35(6):4220–4231.
[32] Lyu ZL, Yang X, Zhang YY, et al. Bi-level optimal strategy of islanded multi-microgrid systems based on optimal power flow and consensus algorithm. Energies. 2020;13(7):1537.
[33] Yousif M, Ai Q, Gao Y, et al. An optimal dispatch strategy for distributed microgrids using PSO. CSEE J Power Energy System. 2020;6(3):724–734.
[34] Bayat P, Afrakhte H. A purpose-oriented shuffled complex evolution optimization algorithm for energy management of multi-microgrid systems considering outage duration uncertainty. J Intell Fuzzy Syst. 2020;38(2):2021–2038.
[35] Yang Y, Qiu J, Qin Z. Multidimensional firefly algorithm for solving day-ahead scheduling optimization in microgrid. J Elect Eng Technol. 2021;16(4):1755–1768.
[36] Yu Y, Gao SC, Cheng S, et al. CBSO: a memetic brain storm optimization with chaotic local search. Memet Comput. 2018;10(4):353–367.
[37] Heidari AA, Mirjalili S, Faris H, et al. Harris hawks optimization: algorithm and applications. Future Gener Comput Syst. 2019;97:849–872.
[38] Mirjalili S, Lewis A. The whale optimization algorithm. Adv Eng Software. 2016;95:51–67.
[39] Mirjalili S, Mirjalili SM, Lewis A. Grey wolf optimizer. Adv Eng Software. 2014;69(3):46–61.
[40] Zhang CL, Ding SF. A stochastic configuration network based on chaotic sparrow search algorithm. Knowledge-Based Syst. 2021;220(10):106924.
[41] Zhang HJ, Feng YB, Lin KP. Application of multi-species differential evolution algorithm in sustainable microgrid model. Sustainability. 2018;10(8):2694.
[42] Wu Y, Lyu L, Xu LX, et al. Optimized allocation of various energy storage capacities in a multi-energy micro-grid considering electrical/thermal/gas coupling demand response. Power Syst Prot Control. 2020;48(16):1–10.
[43] Ye L, Lyu ZL, Wang M, et al. Bi-level programming optimal scheduling of ADN with a multi-microgrid based on optimal power flow. Power Syst Prot Control. 2020;48(18):27–37.
[44] Ding M, Liu XY, Xie JL, et al. Optimal planning model of grid-connected microgrid considering comprehensive performance. Power Syst Prot Control. 2017;45(19):18–26.
[45] He H, Lei X, Huang T, et al. Coordinated and autonomous optimal operation strategy of multi-microgrid system under the guidance of price. Power Syst Prot Control. 2019;47(16):17–26.
[46] Zhou B, Zou JT, Chi YC, et al. Multi-microgrid energy management systems: architecture, communication, and scheduling strategies. <jtl>j Mod Power Syst Clean Energy. 2021;9(3):463–476.
[47] Yang DF, Zhang CX, Jiang C, et al. Interval method based optimal scheduling of regional multi-microgrids with uncertainties of renewable energy. IEEE Access. 2021;9:53292–53305.
[48] Liu YS, Chen X, Li B, et al. State of art of the key technologies of multiple microgrids system. Power Syst Technol. 2020;44(10):3804–3820.
[49] Wang P, Zhang Y, Yang HW. Research on economic optimization of microgrid cluster based on chaos sparrow search algorithm. Comput Intell Neurosci. 2021;2021(3):1–18.